J Mol Model (2009) 15:923–933
DOI 10.1007/s00894-008-0448-z

ORIGINAL PAPER

The effects of light-induced reduction of the photosystem II reaction center

Peter Palencar · Tatyana Prudnikova · Frantisek Vacha · Michal Kuty

Received: 30 October 2008 / Accepted: 15 December 2008 / Published online: 27 January 2009

Abstract Accumulation of reduced pheophytin *a* (Pheo-D1) in photosystem II reaction center (PSII RC) under illumination at low redox potential is accompanied by changes in absorbance and circular dichroism spectra. The temperature dependences of these spectral changes have the potential to distinguish between changes caused by the excitonic interaction and temperature-dependent processes. We observed a conformational change in the PSII RC protein part and changes in the spatial positions of the PSII RC pigments of the active D1 branch upon reduction of Pheo-D1 only in the case of high temperature (298 K) dynamics. The resulting absorption difference spectra of PSII RC models equilibrated at temperatures of 77 K and 298 K were highly consistent with our previous experiments in which light-induced bleaching of the PSII RC absorbance spectrum was observable only at 298 K. These results support our previous hypothesis that Pheo-D1 does not interact excitonically with the other chlorins of the PSII RC, since the reduced form of Pheo-D1 causes absorption spectra bleaching only due to temperature-dependent processes.

Keywords Photosystem II · Reaction center · Pheophytin · Absorption spectra · Exciton interactions · Molecular dynamics

Electronic supplementary material The online version of this article (doi:10.1007/s00894-008-0448-z) contains supplementary material, which is available to authorized users.

P. Palencar · T. Prudnikova · F. Vacha · M. Kuty
Institute of Physical Biology, University of South Bohemia,
Zamek 136,
37333 Nove Hrady, Czech Republic

P. Palencar · M. Kuty (✉)
Institute of Systems Biology and Ecology,
Academy of Sciences of the Czech Republic,
Zamek 136,
37333 Nove Hrady, Czech Republic
e-mail: kuty@ufb.jcu.cz

F. Vacha
Biological Centre, Academy of Sciences of the Czech Republic,
Branisovska 31,
370 05 Ceske Budejovice, Czech Republic

Introduction

Photosystem II (PSII) is one of several protein assemblies that function cooperatively in photosynthesis. Despite great progress in the study of the molecular structure and protein composition of PSII by electron microscopy [1] and X-ray crystallographic analysis, the resolution is not yet sufficient to detect individual atoms [2–6]. As more structural data on PSII become available, new questions arise concerning the nature of the so-called exciton interactions between the PSII reaction center (PSII RC) chlorin pigments (chlorophyll *a* and pheophytin *a*). The exciton interactions (delocalization of the excited states) are caused by dipole–dipole coupling between proximal pigments, and they are important for photosynthetic function in defining the precursor state to the initial charge separation. Such exciton interactions can be essential in the interpretation of experimental results because they can strongly influence the properties of the optical transitions monitored in many studies of photosynthetic complexes. In contrast to bacterial RCs, in which the interaction between two bacteriochlorophylls of a specific pair dominate, there is comparable exciton interaction among core pigments in the PSII RC [7]. Chlorin pigments are collectively responsible for a 'multimeric' absorption band S_0–S_1 (Q_y transition) around 680 nm, which is red-shifted relative to monomeric chlorophylls. Some important details on exciton interactions within chlorin aggregates and

photosynthetic pigment-protein complexes have been revealed by circular dichroism (CD) and absorption spectroscopy, single-molecule spectroscopy, and also from theoretical approaches using molecular structure-based computational models [8–11].

Within the computational approach, some approximations in the molecular exciton model are required. The magnitudes of transition dipoles of chlorophylls, characterizing the transition of ground to low-lying electronic excited states, are quite large and usually it is the lowest electronic transitions, so-called Q_y exciton states, that are of interest because higher excited electronic levels of pigments overlap significantly. The computational molecular structure-based exciton method can be divided into two main computational parts. The first consists of the construction of the Hamiltonian matrix, in which the interaction energies between the molecules (pigments) form non-diagonal matrix elements, whereas individual transition energies of the PSII RC chlorins form diagonal matrix elements. The interaction energies can be calculated by several approaches, but the most popular is the method of point dipole and point-monopole interactions. The point-dipole method [12] concerns the interaction energy between the transition dipole moments, whereas the point-monopole method [13] describes the interaction energy between transition monopoles. Both approximations are popular for their simplicity and also reliability since they provide optical spectra (absorbance, linear and circular dichroism and triplet-singlet difference absorption) comparable with those obtained from experiments [8, 10, 11, 14–19]. The second computational part of the exciton spectra calculation involves matrix diagonalization in order to obtain matrix eigenvectors along with the molecular electric transition dipoles. One may then calculate dipole strength as well as rotational strength (related to absolute molar extinction or absolute molar ellipticity, respectively) for each of the matrix eigenvalues (related to exciton energies). The stick spectra obtained can be completed with Gaussian forms in order to simulate the true inhomogeneously broadened spectra caused by stochastic fluctuations in the protein environment.

The final band shapes of the absorption spectra depend significantly on the relative strength of the energy parameters entered in the Hamiltonian equation. A very important factor affecting the quality of optical spectra calculations is the molecular structure of the system studied. Calculated optical spectra of PSII RC cofactors taken directly from X-ray crystal structures have been very often in good accordance with experimental spectra. However, it has been suggested recently [8] that time- and temperature-dependent processes should be studied on the dynamic 3D molecular structures obtained from molecular dynamics (MD) simulations.

In our previous theoretical study [11], we provided an explanation of our former experimental results [20] concerning reversible bleaching of absorbance and CD spectra upon selective light-induced oxidation of the primary electron donor P680. The effects of the light-induced reduction of the primary electron acceptor pheophytin *a* (Pheo-D1) [20] in the presence of the artificial electron donor sodium dithionite could be also analyzed using a similar theoretical approach. It was observed that, at high temperature (277 K), the resulting absorbance difference and CD spectrum bleaching were much lower compared to primary donor oxidation, and that, at low temperature (77 K), no reversible light-induced change in the CD spectrum was detected. Because of this temperature dependence in the light-induced absorbance and CD changes we have suggested that, at room temperature, reduced Pheo-D1 induces a conformational change in the protein surroundings, and consequently affects the original optical spectra. These charge-induced processes do not occur at low temperature, and therefore the reduced form of Pheo-D1 should not affect the CD and absorbance spectra. This hypothesis is also supported by previous suggestions [18, 21] that charge-induced processes cause conformational changes in protein surroundings, which consequently influence energy transfer and primary charge separation reactions in the PSII RC.

Here, we present a theoretical study on light-induced effects in the PSII RC embedded in a lipid-like membrane, by application of a molecular structure-based model consisting of an exciton model coupled with MD simulations. The equilibrium structure of the PSII RC was negatively charged (reduced) on Pheo-D1 by an electron to observe any possible characteristic bleaching in the absorption difference (neutral minus charged) spectra for the Q_y transition at two significantly different temperatures (77 K and 298 K).

Materials and methods

Model of PSII RC

The initial 3D molecular structure of PSII RC was inferred from X-ray diffraction experiments on PSII isolated from *Thermosynechococcus elongatus* at 3.0 Å resolution (PDB 2AXT) [2]. Our model consists of four large protein subunits of a D1/D2 heterodimer (psbA, psbD) and light-harvesting proteins CP47 and CP43 (psbB, psbC), a heterodimer of cytochrome *b*-559 (psbE, psbF), and nine low-molecular weight membrane subunits (psbH, psbI, psbJ, psbK, psbL, psbM, psbT, psbX and psbZ). Three membrane extrinsic subunits, PsbO, PsbU, and PsbV, interacting with the extended loop regions of D1, D2,

CP43 and CP47 are relatively far from the membrane-associated parts of the PSII RC complex and have not been included in the model. The disulfide bond between D1-Cys 212 and D2-Cys 211 was created, and protonation of His, Asp and Glu residues was predicted by the pKa prediction subroutine in the molecular modeling package YASARA [22, 23]. The carboxyl groups of all Asp and Glu residues were not protonated. Two histidines, CP47-His 157 and CP47-His 201, were protonated at the $N_{\varepsilon 2}$ nitrogen. Twelve histidines, D1-His 92, D1-His 190, D1-His 195, D1-His 337, CP47-His 343, CP43-His 74, CP43-His 91, CP43-His 398, D2-His 61, D2-His 87, D2-His 189 and D2-His 336, were protonated at the $N_{\delta 1}$ and $N_{\varepsilon 2}$ nitrogens. In order to obtain appropriate initial geometries, the remaining His residues were protonated at the $N_{\delta 1}$ nitrogen. Missing N-terminal and C-terminal residues, five isoprene groups of plastoquinone-9 (PQ9) molecules, and some parts of non-protein molecules were modeled using the YASARA and ModLoop server [24]. Hydrogen atoms of the protein part of the PSII RC complex were added automatically by the modeling package WHAT IF or added manually. Chlorin cofactors [six chlorophyll *a* (Chl-*a*) molecules and two pheophytin *a* (Pheo-*a*) molecules] were arranged in the heterodimeric D1/D2 subunits with pseudo-C2 symmetry and are labeled as follows: Chl-*a*-3, Chl-*a*-4, Chl-*a*-5, Chl-*a*-6, Pheo-*a*-7, Pheo-*a*-8, Chl-*a*-9 and Chl-*a*-10. Other cofactors—11 beta-carotenes (β-Car), one non-heme iron, Fe^{2+}, one heme of cytochrome *b*-559 and the Mn_4–Ca cluster (forming the water oxidation catalytic site)—were also included in our model.

Force field parameters of the cofactors

For the protein part of the PSII RC model, the all-atom AMBER99 force field (FF; release 2005) [25] was chosen. However, photosynthetic cofactors, Chl-*a*, Pheo-*a*, heme, β-Car, PQ9, bicarbonate ion (BCT) and the manganese cluster of the oxygen evolving complex (OEC), are not implemented in any extensive bio-molecular FFs, like AMBER [26], CHARMM [27] and Gromos [28]. Fortunately, the molecular structure of these cofactors is very similar to that of bacterial Chl-*a* (BChl-*a*), bacterial Pheo-*a* (BPheo-*a*) and a derivative of ubiquinone, for which AMBER-like FF parameters have been developed [29]. Thus, new FF parameters had to be developed [9] only for structurally different parts like the saturated imidazole ring II on the chlorin macrocycle ring, the vinyl group CH_2=CH– on imidazole ring I, two CO_2–CH_2–CH_2 groups attached to heme, part of the phytyl tail, PQ9 head, isoprene units, double-bonds of β-Car, BCT and the OEC–BCT complex. FF parameters, describing equilibrium values of bonds, angles and dihedral angles and their force constants, were developed by performing a series of quantum mechanics (QM) ab inito calculations at HF/6-31G* level of theory [30] according to the AMBER developing scheme [25]. Partial atom centered point charges for all PSII RC pigments, including the neutral and reduced state of the Pheo-D1 molecule, were developed according to the restrained-electrostatic potential (RESP) method [31] using QM HF/6-31G* calculations.

Preparation of reduced Pheo-D1

Ab initio QM calculations on the charged (reduced) system containing only a Pheo-D1 molecule and 21 surrounding amino acids revealed the charge distribution; 94% of charge from the electron donated to this system was found to be localized on a cyclic part of Pheo-D1, 1% on the rest of the Pheo-D1 atoms, and only 5% on surrounding amino-acids. Therefore, we approximated the light-adapted PSII RC using the equilibrated model of PSII RC (Eq-PSII RC; details on preparation given below), in which the donated electron is fully localized on Pheo-D1. The point atomic charges of Pheo-D1 were placed into the Eq-PSII RC model according to our QM calculations.

Preparation of an equilibrated model of PSII RC

The model of the PSII RC pigment–protein complex[1] was put into the simulation cell with dimensions extended by 1.2 nm along each axis. Final cell dimensions after energy minimization and geometry optimization were 14.82 nm × 12.46 nm × 11.06 nm. This size ensured that no self-interaction of the PSII RC complex would appear during MD simulation. In order to simulate the infinite size of the system and to establish a natural-like density of the whole cell, periodic boundaries were used for cell walls. The natural environment of the PSII RC pigment–protein complex is thylakoid membrane formed by a lipid bilayer surrounded by water solution. The membrane was replaced by an assembly of octane molecules [32–35] due to the lack of electron density for lipid components and computationally demanding geometry optimization of lipid–protein complexes. The middle part of the cell was filled up with octane, while the extrinsic parts of the PSII RC complex, located in the center of the cell, were solvated by water (see Fig. 1). The cavities around D2-PQ9, OEC and the putative water channel were also partially filled with water mole-

[1] Multiple time steps of 1 fs for intramolecular and 2 fs for intermolecular forces was found the most appropriate. A cutoff of 0.8 nm was used for Lennard-Jones and electrostatic interactions. To treat long-range electrostatic interactions outside the cutoff region, the particle mesh Ewald (PME) method [53] with a grid spacing < 0.1nm, 4th order B-splines and a tolerance of 10^{-4} for the direct space sum were used. The temperature was adjusted by Berendsen thermostat [54] based on the time-averaged temperature.

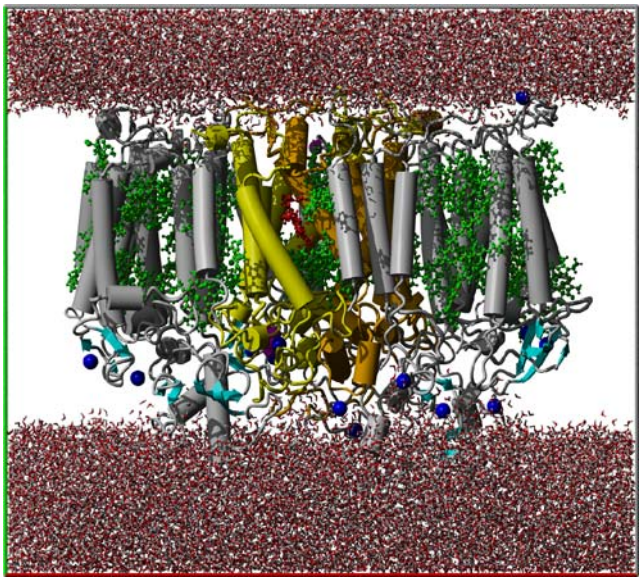

Fig. 1 Equilibrated photosystem II reactive center (Eq-PSII RC) model embedded in a periodic simulation cell. View along the thylakoid membrane with the stromal side of the PSII RC pigment–protein complex heading up. The water layers are located above and below the centered PSII RC complex; water molecules are represented by *red* (oxygen) and *white* (hydrogen) sticks. The protein part of PSII RC is shown as a *gray cartoon model* with *cylinders* and *tubes* representing secondary structure. D1 and D2 protein subunits are colored *yellow* and *orange*, respectively. The non-protein part of PSII RC is shown by *a green* and *magenta* ball-and-stick model. Pheophytins are colored *red*. The octane environment surrounding the PSII RC complex is hidden and only head group atoms of PSII RC pigments are shown for clarity. Counter ions, which are localized mainly at the lumenal surface of the PSII RC complex, are represented as *blue balls*

cules. First, close contacts between the PSII RC pigment–protein complex and octane molecules were allowed to equilibrate by a combination of geometry optimization and further MD optimization. Fixation of positions of all pigment molecules, extrinsic water molecules and Cα backbone carbons was needed to avoid unfavorable conformational changes. After 500 ps of MD simulation, protein subunits and water molecules forming the walls and entering buried PSII RC cavities, were released to move. Octane and water molecules could freely penetrate and fill the cavities. Additional octane molecules gradually entered the system until a natural-like density of octane environment was achieved.

In the next step, extrinsic water molecules were also released to move. An equilibrated contact layer between octane and water was observed after approximately 2 ns simulation. At this point all atoms in the simulation cell were released and MD simulation with a time step of 1.0 fs was used to complete the geometry optimization. The content of the simulation cell was neutralized by 13 sodium cations (by using the automatic procedure for cell neutralization and pKa prediction in YASARA, [22, 23]). The net charge of the cell after correction of two histidines close to the OEC was −2. Except for the last 1 ns of Eq-PSII RC preparation, where NPT ensemble was used, NVT ensemble was used during the whole energy minimization and geometry optimization process. The process was finished when there was no change in dimensions of the simulation cell, and the root-mean-square deviation (RMSD) of positions of PSII RC pigments and Cα carbons fluctuated around values typical of a thermal movement. The total simulation time of the Eq-PSII RC model was approximately 5 ns. The application of relatively small octane molecules ensures their relatively fast equilibration (from 1 to 3 ns) [33], in contrast to complexes containing lipid layers [36, 37], which have a typical equilibration time of 10–20 ns. The final Eq-PSII RC model contained overall 204.680 atoms, including 26.582 water molecules, 2.411 octanes and 13 sodium cations. The resulting Eq-PSII RC model embedded in the simulation cell is shown in Fig. 1.

MD simulations of the Eq-PSII RC model

We performed six various MD simulations on Eq-PSII RC models according to our previous experimental conditions [11, 20]. To account for the wide range of dynamic motions in the Eq-PSII RC model, a 1 fs time step in a 20 ns MD trajectory was chosen. MD simulations on a dark-adapted Eq-PSII RC model with all pigments in neutral form at temperatures 298 K and 77 K were termed Neutral-MD; MD simulations on the light-adapted Eq-PSII RC model, with negative charge on Pheo-D1, were termed $Pheo^{-}$-MD; and MD simulations on the light-adapted Eq-PSII RC model, with slightly different starting conditions from $Pheo^{-}$-MD, were termed collateral-$Pheo^{-}$-MD simulations. A schematic representation of the MD simulations described above, omitting collateral $Pheo^{-}$-MD simulations, is given in Fig. 2.

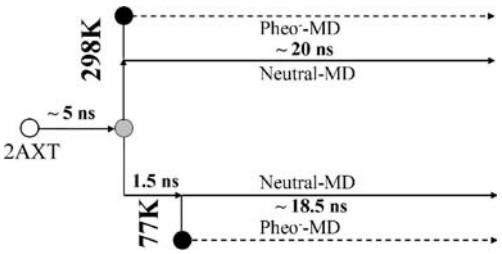

Fig. 2 Schematic representation of initial Eq-PSII RC model preparation and four parallel MD simulations on the dark-adapted and the light-adapted Eq-PSII RC model. *2AXT* X-ray crystal structure of PSII RC [2], *gray circle* Eq-PSII RC model obtained after ~5 ns of energy minimization and geometry optimization, *two black circles* (located at the beginning of the 77K-branch and 298K-branch) points at which Pheo-D1 was reduced. The short, 1.5-ns-long section prior to the 77K-branch illustrates further energy minimization and geometry optimization of the Eq-PSII RC model originally prepared at 298 K. More details are given in the text

Exciton absorption spectra of PSII RC

The spectral properties (absorption spectra) of PSII RC were simulated by a molecular exciton matrix method [38] based on the PSII crystal structure (accession code 2AXT [2] in RCSB Protein Data Bank).

An electronic Hamiltonian for the Frenkel exciton was used, taking only the lowest excited state Q_y into account [39]:

$$H = \sum_{i,j} (E + D_i + \Delta_i)\langle i|i\rangle + V_{ij}\langle i|j\rangle,$$

in which E is the electronic monomer transition energy of non-interacting PSII RC pigment i, D_i is the solvent shift (origin of spectral heterogeneity), and Δ_i is an origin of inhomogeneous broadening of the pigment i caused by stochastic fluctuations in the protein environment. To account for Δ_i as a random shift from average energy $E+D_i$, Gaussian distribution of transition energies represented by diagonal elements of Frenkel Hamiltonian is commonly used. Full-width at half-maximum (FWHM) of 210 cm^{-1} was used following previous finding [7, 16, 40]. A nondiagonal energetic disorder caused by fluctuations of intermolecular interactions could be omitted due to its negligible effect on the spectra [39].

For the dark-adapted PSII RC system (without charge separation on the pigments) the one-exciton Hamiltonian of eight chlorins was given by the matrix containing 8×8 two-pigment coupling energies. The main diagonal consists of the monomer transition energy of pigments (seven Chl-*a* and one Pheo-*a*). The unperturbed site energies of the excited states have been adapted from the linear OD/LD/CD/FL spectra fit based on an evolutionary algorithm [10].

The Hamiltonian matrix for the light-induced PSII RC with negatively charged Pheo-D1 was constructed differently. In order to involve the presence of the reduced form of Pheo-D1, electrochromic shifts in site energies [10] of the remaining PSII RC pigments (Fig. 3) were included and could be computed as the interaction energy between atomic partial charges of Pheo-D1 and differential dipole moments of the excited and ground states of PSII RC pigments. The negative charge that was distributed mostly over the head group atoms of Pheo-D1 molecule (exactly 95% on head group atoms and less than 5% over the atoms in the surrounding environment, according to our QM calculations; data not shown) affects transition energies of all other PSII RC pigments in the ground state. The electrochromic shift of transition energy ΔE was calculated as the interaction energy between all atomic partial charges δq_i of reduced Pheo-D1 and the vector $\Delta\vec{\mu}$ of the pigment in the ground state. The vector $\Delta\vec{\mu} = \vec{\mu}_e - \vec{\mu}_g$, defined as the difference between the permanent dipole moment of the excited and ground state, is oriented approximately in the direction of two nitrogen atoms $N_A \rightarrow N_C$ from the macrocycle head group of chlorophyll [41], and has a magnitude of around 1 Debye. The electrochromic shift is defined by $\Delta E = \left(1/4\pi\varepsilon_{eff}\right)\sum_i \delta q_i\left(\vec{r_i}/r_i^3\right)\Delta\vec{\mu}$, where ε_{eff} is the effective dielectric constant and $\vec{r_i}$ is a vector connecting the center of the PSII RC pigment in the ground state and all atoms from reduced Pheo-D1. A value of ε_{eff} = 1.5 was used in all calculations according to previous similar studies [10]. For simplicity, the oscillator strength and exciton couplings of the reduced form of the Pheo-D1 pigment were neglected.

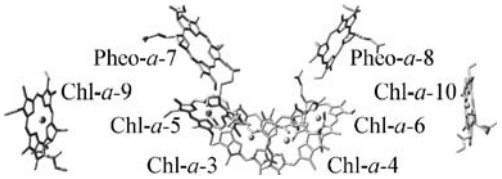

Fig. 3 Nomenclature and spatial organization of PSII RC pigments. Odd-numbered pigments represent active branches and those with even numbers represent inactive branches of the PSII RC complex. The special pair chlorophylls are labeled as Chl-*a*-3 and Chl-*a*-4. Accessory chlorophylls are named Chl-*a*-5 and Chl-*a*-6. Two pheophytins are labeled as Pheo-*a*-7 and Pheo-*a*-8. For reduced Pheo-*a*-7 the abbreviation Pheo-D1 is also used. Chlorophylls Chl-*a*-9 and Chl-*a*-10 represent peripheral chlorophylls. The numbering of pigments was taken from the crystal structure PDB 1S5L [4]. Only chlorin head groups of all pigments are shown for clarity. Pigments are oriented along the plane of the thylakoid membrane with stromal side heading up

The non-diagonal exciton coupling energies V_{ij} were computed by using the transition dipole [19] and also transition monopole methods [13]. The dipole–dipole interaction energy V_{ij} (in cm^{-1}) between transition dipole moments of pigments is defined by:

$$V_{ij} = \frac{5.04}{\varepsilon}\left[\frac{\vec{\mu}_i \cdot \vec{\mu}_j}{r_{ij}^3} - \frac{3\left(\vec{r_{ij}} \cdot \vec{\mu_i}\right)\left(\vec{r_{ij}} \cdot \vec{\mu_j}\right)}{r_{ij}^5}\right],$$

where ε is a dielectric constant and $\vec{\mu}_i$ is the transition dipole moment (in Debye), Q_y transition dipoles were assumed to be oriented from the N_A atom (on pyrrole ring I) to the N_C atom (on pyrrole ring III) of the chlorophyll molecules and $\vec{r}_{ij}$ is the vector connecting the centers of the *i*-th and *j*-th PSII RC pigments (in nm).

The interaction energy within the transition monopole approximation [42] is expressed by the sum of the Coulomb interactions of all transition monopoles. The non-diagonal interaction matrix elements are calculated as:

$$V_{ila,jlb} = \sum_n \sum_m \frac{q_{inla} q_{jmlb}}{R_{in,jm}},$$

where q_{inla} is transition monopole n associated with the transition $l \rightarrow a$ on chromophore i, and $R_{in,jm}$ is the distance between monopoles *in* and *im*. The values of transition

monopole charges for Chl *a* and Pheo-*a* were obtained from published data [13].

Formally, it is also advisable to improve Hamiltonian by involving the influence of charge-transfer (CT) transitions [43, 44] in which an electron from a ground state of one molecule is transferred to an excited state of another. However, the optical absorption of CT states is often weak and usually masked by vibronic replicas of Frenkel states [45]. According to previous similar studies, several other effects, such as simultaneous excitation of more than one reaction center chlorin, and electron-phonon coupling, could be also neglected in the exciton Hamiltonian.

In the next step, we diagonalized Hamiltonian represented by a matrix H_{ij} to find its eigenvalues and eigenvectors. The energies of the PSII RC exciton states are given by the eigenvalues of Hamiltonian, whereas the components of the corresponding normalized eigenvectors specify the amplitude of each pigment's contribution to each exciton state. The resulting steady-state optical spectra arising from these eigenvalues and eigenvectors were calculated as follows [19].

The intensity of a spectral band is proportional to the so-called dipole strength, which is the transition dipole moment squared, μ^2. Dipole strengths of the particular exciton states k were calculated as:

$$\mu_k^2 = \sum_{i,j}^{n} \left(\vec{\mu}_i \cdot \vec{\mu}_j \right) U_{ik} U_{jk},$$

where U_{ik} and U_{jk} are corresponding eigenvectors [18]. Position vectors $\vec{r}_{ij}$ and the orientation of the dipole moments $\vec{\mu}_i$ were taken from selected MD snapshots holding equilibrated dynamic structures of PSII RC (for more details see Results and discussion). Monomer transition energies of PSII RC pigments for the Q_y transition were taken from recently published data [10]. Transition dipole strengths of 23 and 14 Debye^2 for Chl-*a* and Pheo-*a*, respectively, were used [7, 16]. The stick spectra were then completed with Gaussian forms. Each of the envelopes has the FWHM of 150 cm^{-1}, which corresponds roughly to the homogenous line-width of Chl-*a* at room temperature [46]. An ensemble averaging over 10.000 RC spectra generated the presented plots of oscillator strength against wavelength for the exciton states of PSII RC.

Software and hardware facilities

The non-diagonal Hamiltonian matrix elements (within transition monopole and dipole approximation), eigenvectors and eigenvalues were calculated using the mathematical software package MATLAB [47]. All QM calculations concerning molecular geometry optimizations and FF parameter development were performed using Gaussian 98 [48]. The AMBER-like atomic partial RESP charges were obtained by Antechamber, which is an accessory module of AMBER version 7 [49]. Hydrogenation of PSII RC protein was performed by WHAT IF [50]. For viewing and rendering of a molecular structure, protein solvation in periodic cell, MD simulations and MD trajectory analysis, RasMol [51], GROMACS [52], and YASARA [22, 23] software packages were applied. MD simulations in YASARA (version 8.10.30) and QM calculations in Gaussian 98 were carried out on a high-performance parallel computing cluster (Beowulf design).

Results and discussion

Light-induced conformational changes

The conformational changes close to the position of reduced Pheo-D1 have been evaluated in Pheo$^-$-MD simulations by the RMSD of Cα carbons positions within the D1 and D2 protein subunits. The X-ray crystal structure of PSII (PDB ID 2AXT) was used as a reference structure for all Cα RMSD calculations. Translation and rotation of the PSII RC complex in the simulation cell was eliminated during MD simulations by using superimposition. To gain more detail about the conformational changes within MD simulations, three protein shells of the Eq-PSII RC model were selected at different distances from the Pheo-D1 head group. The first protein shell, within 0.23 nm of the Pheo-D1 head group (marked as 0.23 nm-Cα layer), involves amino acids D1-Tyr 126, D1-Gln 130, D1-Tyr 147, D1-Val 283, D2-Leu 205, D2-Leu 209 and D2-Ala 212. The second protein shell, defined within the distance range of 0.23 nm–0.5 nm from the Pheo-D1 head group (0.5 nm-Cα layer) involves D1-Ile 143, D1-Ala 146, D1-Ala 149, D1-Pro 150, D1-Val 205, D1-Pro 279, D1-Val 280, D2-Ala 208, D2-Cys 211, D2-Ile 213, D2-Ala 216, D2-Trp 253, D2-Ile 256 and D2-Phe 257. The last protein shell (0.7 nm-Cα layer) contains 24 amino acids of D1 and 13 amino acids of the D2 protein subunit. The results of conformational analysis of Neutral-MD and Pheo$^-$-MD simulations at 298 K for selected protein shells are shown in Fig. 4. For better readability, a polynomial fit was applied to all of the Cα RMSD raw data (the RMSD raw data with related polynomial fits is depicted in Fig. S1a and b). It is evident that the Cα RMSD of the protein increases with distance from Pheo-D1 head group because of thermal movement within interior of the protein, particularly in the D1 protein subunit. Small conformational changes detected at 298 K for Neutral-MD result from thermal movements and those are given here as reference data. The shape of Cα RMSD plots obtained from 298 K Pheo$^-$-MD provides reasonable evidence that the equilibrated light-adapted Eq-PSII RC

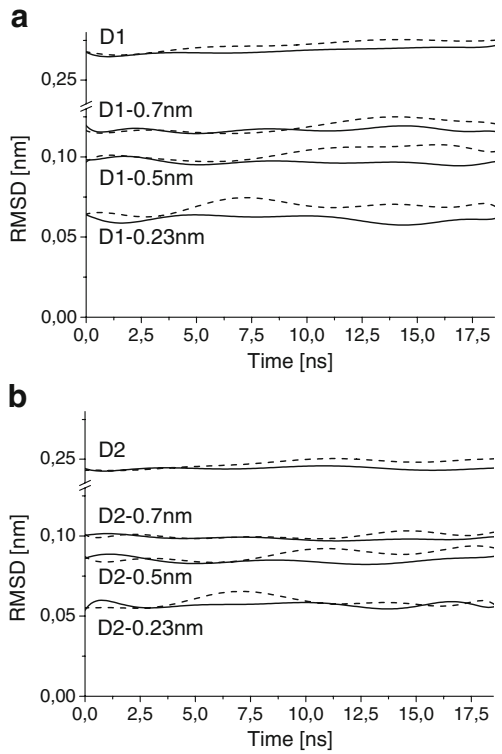

Fig. 4 Conformational analysis of Neutral-MD simulations (*solid lines*) and Pheo$^-$-MD (*dashed lines*) at 298 K performed on selected spherical protein layers of Eq-PSII RC model. **a** Root mean square deviations of alpha carbons (Cα RMSD) of the whole D1 protein subunit, Cα RMSD of D1 spherical layers that differ by increasing distance from Pheo-D1 head group (the first layer within 0.00–0.23 nm from Pheo-D1, the second layer within 0.23–0.5 nm, and finally the third layer within 0.50–0.70 nm). **b** Cα RMSD of the D2 protein subunit, and Cα RMSD of protein layers of D2 that differ by increasing distance from Pheo-D1 head group (layers as in **a**). For better readability, a polynomial fit (9th order) was applied to all Cα RMSD raw data

model has changed its conformation slightly within both D1 and D2 subunits, particularly in proximity to reduced Pheo-D1.

We have also evaluated the spatial orientation and position of PSII RC chlorin pigments (shown in Fig. 3) within MD simulations by a RMSD of N_A (on pyrrole ring I) and N_C (on pyrrole ring III) chlorin atoms. The results from N_A-RMSD and N_C-RMSD analysis of the pigment part of the light-adapted Eq-PSII RC model obtained from Pheo$^-$-MD simulation at 298 K and 77 K are shown in Fig. 5. For all N_A-RMSD and N_C-RMSD calculations, the equilibrated molecular geometry of PSII RC pigments of the dark-adapted Eq-PSII RC model was used as a reference structure. Due to the 9th order polynomial fit applied to all RMSD graphs (the RMSD raw data with related polynomial fits depicted in Fig. S2), the zero values of all N_A-RMSD and N_C-RMSD at 0 ns cannot be seen. Figure 5 consists of two main parts, the first (Fig. 5a) shows the N_A-RMSD and N_C-RMSD plot at 298 K, and the second (Fig. 5b) at 77 K. The first column shows the results of conformational analysis of particular PSII RC pigments from the active branch, and the second column results from the inactive branch, respectively. Values of N_A-RMSD and N_C-RMSD fluctuating around 0.05 nm could be assigned to thermal movements typical of these types of atoms at 298 K [8]; however, changes in positions of PSII RC pigments were also detected. Not surprisingly, major changes have been observed for PSII RC pigments from the active branch at both temperatures. Accessory chlorophyll Chl-*a*-5, which is the pigment closest to reduced Pheo-D1, exhibits considerable change during 298K-Pheo$^-$-MD. No substantial

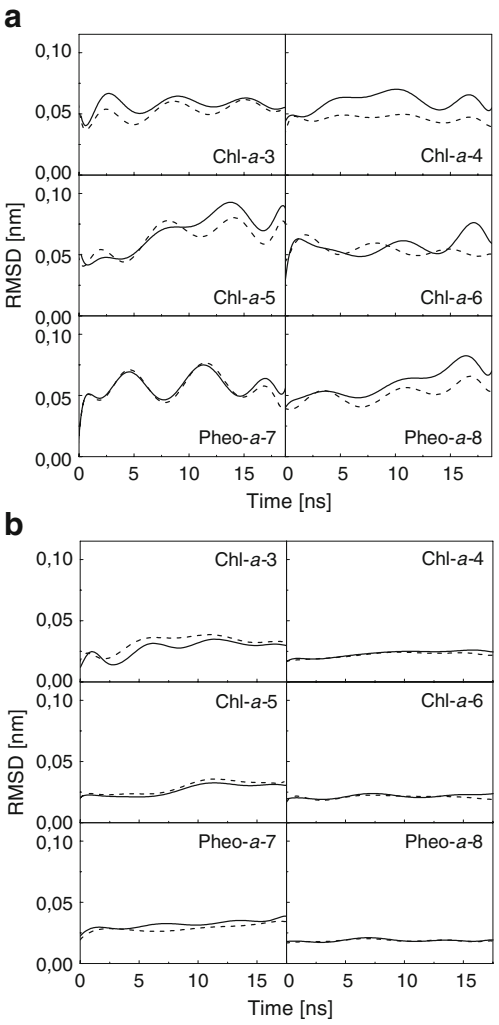

Fig. 5 Conformational analysis (RMSD plots) of Pheo$^-$-MD simulations on N_A (*solid lines*) and N_C (*dashed lines*) atoms of PSII RC chlorins, at **a** 298 K and **b** 77 K. For better readability only, a polynomial fit (9th order) was applied to all of the N_A-RMSD and N_C-RMSD raw data. Both plots consist of two columns; the first exhibits the results of a conformational analysis of the PSII RC pigments from the active, D1 branch, and the second results from the inactive, D2 branch

rotations of head groups of PSII RC pigments were observed except for peripheral Chl-*a*-9 (not shown). In the case of 77K-Pheo$^-$ -MD, values of N_A-RMSD and N_C-RMSD fluctuated around 0.025 nm, which is typical of thermal movements of these types of atoms at 77 K. Figure 6 illustrates the detected position change of PSII RC pigments (Fig. 3) and D1 protein environment surrounding PSII RC pigments of the active branch during 298K-Pheo$^-$-MD.

We have summarized the results presented in Fig. 5 by calculating weighted average RMSD of PSII RC pigments at 298 K and at 77 K. First, an average value of N_A-RMSD and N_C-RMSD of six PSII RC pigments, Chl-*a*-3, Chl-*a*-4, Chl-*a*-5, Chl-*a*-6, Pheo-*a*-7 and Pheo-*a*-8 was calculated. Next, weighted average RMSDs of peripheral chlorophylls Chl-*a*-9 and Chl-*a*-10 were calculated by using factor 0.5 to account for their smaller exciton coupling to the rest of the PSII RC pigments. Considering both average RMSD values, the final average value of RMSD of PSII RC pigments was obtained. In the case of 298K-Pheo$^-$-MD, the biggest position change of PSII RC pigments was observed during the first 3 ns; after 8.2 ns, the positions of the PSII RC pigments stabilized and an equilibrated system was established. The biggest position change of PSII RC pigments in the case of 77K-Pheo$^-$MD was detected during the first 6.3 ns, and after equilibrating the system for 11.4 ns. The average 77K-RMSD plot was of much lower magnitude when compared to the average 298K-RMSD plot and thus reduction of Pheo-D1 at 77 K did not significantly affect mutual positions and orientations of PSII RC pigments. Thus, the 3D position change of PSII RC pigments and the conformational change in the protein part of the PSII RC complex could be observed only in the case of 298K-Pheo$^-$-MD.

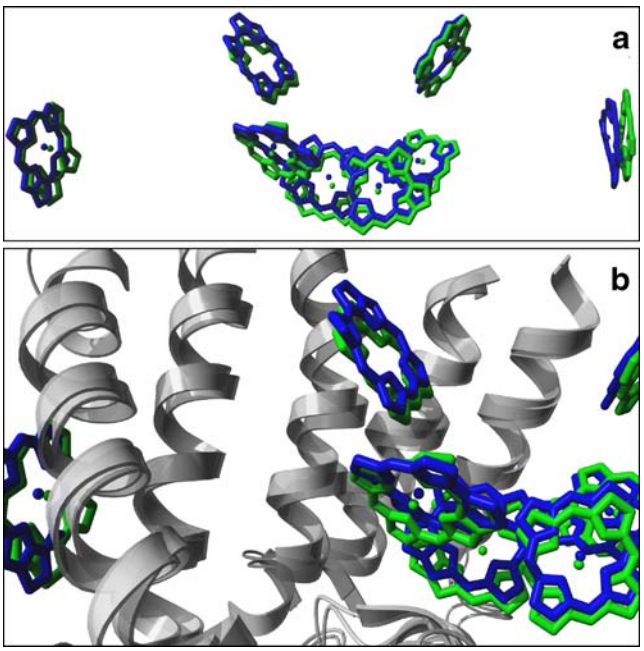

Fig. 6 Conformational changes in pigment and protein environment in PSII RC upon Pheo-D1 reduction at 298 K. **a** Changes in positions of PSII RC pigments. **b** Detailed insight in the vicinity of the active branch of PSII RC. Dynamic structures of PSII RC pigments colored in *green* were obtained from 298K-Neutral-MD and those colored in *blue* from 298K-Pheo$^-$MD (developed after 8.2 ns simulation). Protein backbone of D1 subunit is shown as a *gray ribbon*. Other PSII RC protein subunits are hidden and only chlorin head groups of PSII RC pigments are shown for clarity. The pigments are oriented as in Fig. 3

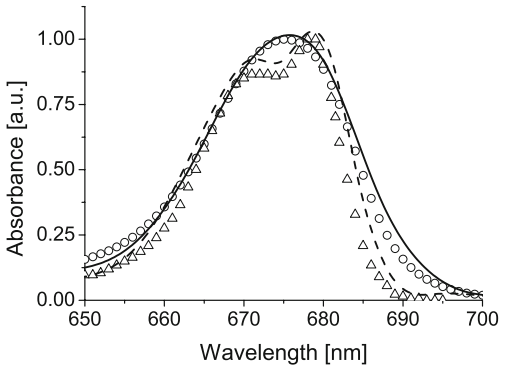

Fig. 7 Comparison of calculated dark-adapted absorption spectra of PSII RC pigments developed by Neutral-MD simulation at 298 K (*solid line*) and 77 K (*dashed line*) with experimental dark-adapted absorption spectra of PSII RC measured at 273 K (*circles*) and 77 K (*triangles*) [11]. For clarity, only spectra calculated with inclusion of inhomogeneous broadening are shown. All spectra are normalized to their maxima using arbitrary units

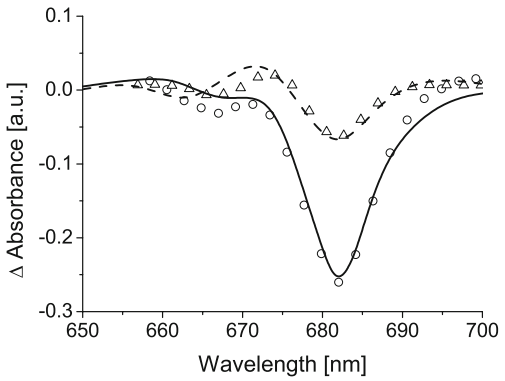

Fig. 8 Comparison of calculated difference (dark minus light-adapted) absorption spectra of PSII RC pigments [developed from Neutral-MD and Pheo$^-$-MD at 298 K (*solid line*) and at 77 K (*dashed line*)] with experimental difference absorption spectra of PSII RC measured at 277 K (*circles*) and 77 K (*triangles*) [20]. For clarity, only those spectra calculated with inclusion of inhomogeneous broadening and electrochromic shift (applicable for light-adapted spectra) are shown. The spectra were normalized using arbitrary units, maintaining the ratio between the minimum peak of the 298K-plot and the minimum peak of the 77K-plot

Absorption spectra of PSII RC pigments

Optical spectra of PSII RC are sensitive to changes in the mutual positions of transition dipole moments of the pigments. According to several previous studies, the vector of the transition dipole moment of the Q_y transition for Chl-*a* and Pheo-*a* pigments has almost the same orientation as a vector connecting N_A to the N_C atom. The molecular coordinates of PSII RC pigments (Fig. 3) were taken by averaging coordinates extracted from MD snapshots in order to calculate dark-adapted and light-adapted absorption spectra. In the case of the 298 K-light-adapted absorption spectrum, an 8.2 ns snapshot of 298K-Pheo$^-$-MD simulation was applied. For a 77 K-light-adapted absorption spectrum, an 11.4 ns snapshot of 77K-Pheo$^-$-MD was used. In order to minimize thermal fluctuations of coordinates of PSII RC pigments, we applied short energy minimization to the whole Eq-PSII RC complex.

A comparison of calculated absorption spectra from Neutral-MD and experimental dark-adapted absorption spectra of PSII RC [11] is shown in Fig. 7. Clearly, both calculated 298 K-plot and 77 K-plot share the same spectral features with both experimental analogs [11]. The position of maximum peak of calculated 298 K-plot at 675.7 nm is almost identical with position of maximum peak of experimental 273 K-plot at 675.2 nm. The two peaks of calculated 77 K-plot at 671.5 nm and 678.6 nm are also in good accordance with the peaks of the experimental 77 K-plot at 672.0 nm and 678.5 nm. Small differences in the shape of the calculated and experimental dark-adapted absorption spectra are the slightly higher intensity of the 77 K-graph maximum at 671.5 nm, and small blue and red shifts of the envelopes of both calculated graphs. We can state that the positions and orientations of PSII RC pigments developed during Neutral-MD simulations at 298 K and 77 K were equilibrated, and that their dark-adapted absorption spectra were almost identical to their experimental analogs.

The difference absorption spectra of PSII RC pigments developed from Neutral-MD and Pheo$^-$-MD at 298 K and 77 K were compared with the experimental difference absorption spectra of PSII RC measured at 277 K and 77 K [20] (see Fig. 8). A considerable bleaching of the absorption spectra observed experimentally at 277 K is comparable with our computed difference absorption spectra at 298 K. The position of the absorbance minimum peak of the calculated 298 K spectrum at 681.9 nm is almost identical with those of the experimental 277 K-graphs at 682.0 nm. The blue shoulder of the calculated 298 K-graphs at 667.8 nm is slightly shifted compared to the blue shoulder of experimental 277 K-graphs at 666.9 nm. Two peaks of the calculated 77 K-graphs at 662.4 nm and 681.8 nm are in accordance with two peaks of the experimental 77 K-graph at 666.7 nm and 682.1 nm, respectively. Differences in shape between the calculated and experimental difference absorption spectra could be explained by the limits of MD and also point-dipole approximation, which does not consider coupling of Q_y to higher excited states.

Summary

Conformational changes in the protein part of PSII RC upon reduction of Pheo-D1 were detected only in the case of high temperature dynamics (298K-Pheo$^-$-MD). Changes in position and orientation of particular PSII RC pigments during 298K-Pheo$^-$-MD were also observed. Significant conformational changes were detected only for interior parts of the D1 protein in proximity to Pheo-D1. The spatial positions of the PSII RC pigments from the active D1 branch changed more then their symmetrically located PSII RC pigments from the inactive branch within 298K-Pheo$^-$-MD and also 77K-Pheo$^-$-MD simulations.

The resulting absorption difference spectra of PSII RC models equilibrated at temperatures of 77 K and 298 K were highly consistent with our previous experiments in which light-induced bleaching of the PSII RC absorbance spectrum was observable only at 298 K. Since temperature does not influence excitonic interaction, the temperature dependence of absorption spectra bleaching upon Pheo reduction does not support a model wherby Pheo-D1 excitonically interacts with other chlorins of the PSII RC.

Acknowledgments Support from the Institutional Research Concept of the Academy of Science of the Czech Republic (AVOZ60870520 and AV0Z50510513) and from the Ministry of Education of the Czech Republic (LC 06010 and MSM6007665808) and the Grant Agency of the Czech Republic (203/08/0114) is gratefully acknowledged.

References

1. Rhee KH, Morris EP, Barber J, Kuhlbrandt W (1998) Three-dimensional structure of the plant photosystem II reaction centre at 8 A resolution. Nature 396(6708):283–286
2. Loll B, Kern J, Saenger W, Zouni A, Biesiadka J (2005) Towards complete cofactor arrangement in the 3.0A resolution structure of photosystem II. Nature 438(7070):1040–1044
3. Biesiadka J, Loll B, Kern J, Irrgang KD, Zouni A (2004) Crystal structure of cyanobacterial photosystem II at 3.2 angstrom resolution: a closer look at the Mn-cluster. Phys Chem Chem Phys 6(20):4733–4736
4. Ferreira KN, Iverson TM, Maghlaoui K, Barber J, Iwata S (2004) Architecture of the photosynthetic oxygen-evolving center. Science 303(5665):1831–1838
5. Kamiya N, Shen JR (2003) Crystal structure of oxygen-evolving photosystem II from *Thermosynechococcus vulcanus* at 3.7-A resolution. Proc Natl Acad Sci USA 100(1):98–103

6. Zouni A, Witt H-T, Kern J, Fromme P, Krauss N, Saenger W, Orth P (2001) Crystal structure of photosystem II from *Synechococcus elongates* at 3.8 Å resolution. Nature 409:739–743
7. Durrant JR, Klug DR, Kwa SL, van Grondelle R, Porter G, Dekker JP (1995) A multimer model for P680, the primary electron donor of Photosystem II. Proc Natl Acad Sci USA 92 (11):4798–4802
8. Vasil'ev S, Bruce D (2006) A protein dynamics study of Photosystem II: the effects of protein conformation on reaction center function. Biophys J 90(9):3062–3073
9. Palencar P, Vacha F, Kuty M (2005) Force field development on pigments of photosystem 2 reaction centre. Photosynthetica 43 (3):417–420
10. Raszewski G, Saenger W, Renger T (2005) Theory of optical spectra of photosystem II reaction centers: location of the triplet state and the identity of the primary electron donor. Biophys J 88 (2):986–998
11. Vacha F, Psencik J, Kuty M, Durchan M, Siffel P (2005) Evidence for localization of accumulated chlorophyll cation on the D1-accessory chlorophyll in the reaction centre of Photosystem II. Photosynth Res 84:297–302
12. Prokhorenko VI, Steensgaard DB, Holzwarth AR (2003) Exciton theory for supramolecular chlorosomal aggregates: 1. Aggregate size dependence of the linear spectra. Biophys J 85(5):3173–3186
13. Chang JC (1977) Monopole effects on electronic excitation interactions between large molecules. I. Application to energy transfer in chlorophylls. J Chem Phys 67(9):3901–3909
14. Barter LMC, Durrant JR, Klug DR (2003) A quantitative structure-function relationship for the Photosystern II reaction center: supermolecular behavior in natural photosynthesis. Proc Natl Acad Sci USA 100:946–951
15. Psencik J, Ma YZ, Arellano JB, Hala J, Gillbro T (2003) Excitation energy transfer dynamics and excited-state structure in chlorosomes of chlorobium phaeobacteroides. Biophys J 84 (2):1161–1179
16. Jankowiak R, Hayes JM, Small GJ (2002) An excitonic pentamer model for the core Q(y) states of the isolated photosystem II reaction center. J Phys Chem B 106(34):8803–8814
17. Renger T, Marcus RA (2002) Photophysical properties of PS-2 reaction centers and a discrepancy in exciton relaxation times. J Phys Chem B 106(7):1809–1819
18. Dekker JP, Van Grondelle R (2000) Primary charge separation in Photosystem II. Photosynth Res 63(3):195–208
19. Pearlstein RM (1991) Theoretical interpretation of antenna spectra. In: Scheer H (ed) Chlorophylls. CRC, Bocca Raton, FL, pp 1047–1078
20. Vacha F, Durchan M, Siffel P (2002) Excitonic interactions in the reaction centre of Photosystem II studied by using circular dichroism. Biochim Biophys Acta 1554:147–152
21. Konermann L, Gatzen G, Holzwarth AR (1997) Primaryrocesses and structure of the photosystem II reaction center. 5. Modeling of the fluorescence kinetics of the D1-D2-cyt-b559 complex at 77 K. J Phys Chem B 101:2933–2944
22. Krieger E, Darden T, Nabuurs SB, Finkelstein A, Vriend G (2004) Making optimal use of empirical energy functions: force-field parameterization in crystal space. Proteins 57(4):678–683
23. Yasara Biosciences, available via http://www.yasara.org/index.html
24. ModLoop server, available via http://alto.compbio.ucsf.edu/modloop/modloop.html
25. Cornell WD, Cieplak P, Bayly CI, Gould IR, Merz KM, Ferguson DM, Spellmeyer DC, Fox T, Caldwell JW, Kollman PA (1995) A 2nd generation force-field for the simulation of proteins, nucleic acids, and organic-molecules. J Am Chem Soc 117(19):5179–5197
26. Wang JM, Cieplak P, Kollman PA (2000) How well does a restrained electrostatic potential (RESP) model perform in calculating conformational energies of organic and biological molecules? J Comp Chem 21(12):1049–1074
27. MacKerell AD, Bashford D, Bellott M, Dunbrack RL, Evanseck JD, Field MJ, Fischer S, Gao J, Guo H, Ha S, Joseph-McCarthy D, Kuchnir L, Kuczera K, Lau FTK, Mattos C, Michnick S, Ngo T, Nguyen DT, Prodhom B, Reiher WE, Roux B, Schlenkrich M, Smith JC, Stote R, Straub J, Watanabe M, Wiorkiewicz-Kuczera J, Yin D, Karplus M (1998) All-atom empirical potential for molecular modeling and dynamics studies of proteins. J Phys Chem B (102):3586–3616
28. vanGunsteren WF, Daura X, Mark AE (1998) GROMOS force field. In: Encyclopaedia of Computational Chemistry 2. CRC, Boca Raton, pp 1211–1216
29. Ceccarelli M, Procacci P, Marchi M (2003) An ab initio force field for the cofactors of bacterial photosynthesis. J Comput Chem 24 (2):129–142
30. Roothaan CCJ (1951) New developments in molecular orbital theory. Rev Mod Phys 23(2):69–89
31. Bayly CI, Cieplak P, Cornell WD, Kollman PA (1993) A well-behaved electrostatic potential based method using charge restraints for deriving atomic charges: the RESP model. J Phys Chem 97(40):10269–10280
32. Matyus E, Monticelli L, Kover KE, Xu Z, Blasko K, Fidy J, Tieleman DP (2006) Structural investigation of syringomycin-E using molecular dynamics simulation and NMR. Eur Biophys J 35 (6):459–467
33. Stockner T, Ash WL, MacCallum JL, Tieleman DP (2004) Direct simulation of transmembrane helix association: role of asparagines. Biophys J 87(3):1650–1656
34. Aliste MP, MacCallum JL, Tieleman DP (2003) Molecular dynamics simulations of pentapeptides at interfaces: salt bridge and cation-pi interactions. Biochemistry 42(30):8976–8987
35. Tieleman DP, Berendsen HJ, Sansom MS (2001) Voltage-dependent insertion of alamethicin at phospholipid/water and octane/water interfaces. Biophys J 80(1):331–346
36. Tieleman DP (2006) Computer simulations of transport through membranes: passive diffusion, pores, channels and transporters. Clin Exp Pharmacol Physiol 33(10):893–903
37. MacCallum JL, Tieleman DP (2006) Computer simulation of the distribution of hexane in a lipid bilayer: spatially resolved free energy, entropy, and enthalpy profiles. J Am Chem Soc 128 (1):125–130
38. Bayley PM (1973) The analysis of circular dichroism of biomolecules. Prog Biophys 27:1–76
39. Pullerits T (2000) Exciton states and relaxation in molecular aggregates: Numerical study of photosynthetic light harvesting. J Chin Chem Soc 47:773–784
40. Prokhorenko VI, Holzwarth AR (2000) Primary processes and structure of the photosystem II reaction center: a photon echo study. J Phys Chem B 104(48):11563–11578
41. Krawczyk S (1991) Electrochromism of chlorophyll-a monomer and special-pair dimer. Biochim Biophys Acta 1056 (1):64–70
42. Sauer K, Cogdell RJ, Prince SM, Freer A, Isaacs NW, Scheer H (1996) Structure-based calculations of the optical spectra of the LH2 bacteriochlorophyll-protein complex from *Rhodopseudomonas acidophila*. Photochem Photobiol 64(3):564–576
43. Warshel A, Parson WW (1987) Spectroscopic properties of photosynthetic reaction centers. I. Theory. J Am Chem Soc 109: 6143–6152
44. Parson WW, Warshel A (1987) Spectroscopic properties of photosynthetic reaction centers. II. Application of the theory to *Rhodopseudomonas viridis*. J Am Chem Soc 109:6152–6163

45. Petelenz P (2004) Charge-transfer interactions—their manifestations in electroabsorption spectra. J Lumin 110(4):325–331
46. Konermann L, Holzwarth AR (1996) Analysis of the absorption spectrum of photosystem II reaction centers: temperature dependence, pigment assignment, and inhomogeneous broadening. Biochemistry 35(3):829–842
47. MATLAB, http://www.mathworks.com/products/matlab/requirements.html
48. Frisch MJ, Trucks GW, Schlegel HB, Scuseria GE, Robb MA, Cheeseman JR, Zakrzewski VG, Montgomery JA, Stratmann RE, Burant JC, Dapprich S, Millam JM, Daniels AD, Kudin KN, Strain MC, Farkas O, Tomasi J, Barone V, Cossi M, Cammi R, Mennucci B, Pomelli C, Adamo C, Clifford S, Ochterski J, Petersson GA, Ayala PY, Cui Q, Morokuma K, Malick DK, Rabuck AD, Raghavachari K, Foresman JB, Cioslowski J, Ortiz JV, Stefanov BB, Liu G, Liashenko A, Piskorz P, Komaromi I, Gomperts R, Martin RL, Fox DJ, Keith T, Al-Laham MA, Peng CY, Nanayakkara A, Gonzalez C, Challacombe M, Gill PMW, Johnson BG, Chen W, Wong MW, Andres JL, Head-Gordon M, Replogle ES, Pople JA (1998) Gausian 98. Gaussian, Pittsburgh
49. Case DA, Pearlman DA, Caldwell JW, Cheatham TE 3rd, Wang J, Ross WS, Simmerling CL, Darden TA, Merz KM, Stanton RV, Cheng AL, Vincent JJ, Crowley M, Tsui V, Gohlke H, Radmer RJ, Duan Y, Pitera J, Massova I, Seibel GL, Singh UC, Weiner PK, Kollman PA (2002) AMBER 7, University of California, San Francisco
50. Vriend G (1990) WHAT IF: a molecular modeling and drug design program. J Mol Graph 8(1):52–56
51. Sayle RA, Milner-White EJ (1995) RASMOL: biomolecular graphics for all. Trends Biochem Sci 20(9):374
52. Lindahl E, Hess B, van der Spoel (2001) GROMACS: a package for molecular simulation and trajectory analysis. J Mol Model 7:306–317
53. Essmann U, Perera L, Berkowitz ML, Darden T, Lee H, Pedersen LG (1995) A smooth particle mesh Ewald method. J Chem Phys 103(19):8577–8593
54. Berendsen HJC, Postma JPM, vanGunsteren WF, DiNola A, Haak JR (1984) Molecular dynamics with coupling to an external bath. J Chem Phys 81(8):3684–3690